Biophotonics research in Riga: recent projects and results

Spigulis, Janis, Kuzmina, Ilona, Lihacova, Ilze, Lukinsone, Vanesa, Cugmas, Blaž, et al.

Janis Spigulis, Ilona Kuzmina, Ilze Lihacova, Vanesa Lukinsone, Blaž Cugmas, Andris Grabovskis, Edgars Kviesis-Kipge, Alexey Lihachev, "Biophotonics research in Riga: recent projects and results," Proc. SPIE 11585, Biophotonics—Riga 2020, 1158502 (28 October 2020); doi: 10.1117/12.2581799

SPIE.

Event: Third International Conference Biophotonics Riga 2020, 2020, Riga, Latvia

Biophotonics research in Riga: recent projects and results

Janis Spigulis*, Ilona Kuzmina, Ilze Lihacova, Vanesa Lukinsone, Blaž Cugmas, Andris Grabovskis, Edgars Kviesis-Kipge and Alexey Lihachev

Biophotonics Laboratory, Institute of Atomic Physics and Spectroscopy, University of Latvia
Raina Blvd 19, Riga, LV-1586, Latvia

ABSTRACT

A brief review on the activities of Biophotonics Laboratory at UL Institute of Atomic Physics and Spectroscopy, following the previous *Biophotonics Riga - 2017* conference, is presented. Twelve recent research projects are considered, including two EC Horizon-2020 projects, six European Regional Development Fund projects and four projects funded by the Latvian Council of Science. The projects are generally aimed at development of new optical methods and technologies for noninvasive in-vivo skin assessment to facilitate early diagnostics of skin malformations (including cancers), sepsis and cutaneous blood microcirculation features. Most of the projects explore novel approaches of camera-based biomedical imaging for clinical diagnostics and recovery monitoring.
Keywords: optical diagnostics, multi-spectral and fluorescence imaging, chromophore mapping, veterinary biophotonics

1. INTRODUCTION

This review gives insight in some results achieved at the Biophotonics Laboratory in Riga over the years 2018-2020, i.e. after the recent *Biophotonics - Riga* conference held in August, 2017 [1]. Twelve most important research projects are considered, some of them completed during this period and some still running.

Projects funded by the European Commission:

1. H2020 #871124 *Laserlab-Europe*, sub-project *BIOAPP*, D33.16 *"Multi-modal time-resolved laser excited imaging technique for selective analysis of tissue individual fluorophores"* (completed 2019).
2. H2020 #745396-DogSPEC-H2020-MSCA-IF-2016 "*Multimodal spectral imaging for assessment of dog skin erithema: from lab to clinic – DogSpec"* (completed 2020).
3. ERDF #1.1.1.1/16/A/065 "*Optical noninvasive hybrid method for early diagnostics of sepsis and therapy management"* (completed 2019).
4. ERDF #1.1.1.1/16/A/197 "*Portable device for early non-contact diagnostics of skin cancer"* (completed 2019).
5. ERDF #1.1.1.1/18/A/132 "*Multimodal imaging technology for in-vivo diagnostics of skin malformations* (running).
6. ERDF #1.1.1.2/VIAA/1/16/014 "*Time-resolved autofluorescence methodology for non-invasive diagnostics of skin cancer"* (running).
7. ERDF #1.1.1.2/VIAA/1/16/052 "*Development and clinical validation of a novel cost effective multi-modal methodology for early diagnostics of skin cancers"* (running).
8. ERDF #1.1.1.2/VIAA/1/16/070 "*Development of prototype devices for nonivasive assessment of skin condition"* (running).

Projects funded by the Latvian Council of Science:

1. # lzp-2018/1-0188 *"Photoplethysmography imaging for assessment of chronic pain"* (running).
2. # lzp-2018/2-0052 *"Improving the early diagnosis of skin cancer with neural networks"*(running).
3. # lzp-2018/2-0051*" Fast and non-contact optical estimation of microorganisms activity."* (running).
4. # lzp-2018/2-0006 *"Advanced spectral imaging technology for skin diagnostics"* (running).

Administrative details on these projects can be found at https://www.asi.lu.lv/en/labs/biophotonics-laboratory/. Here we will focus mainly on the results of already completed projects. For compactness, references to the projects below will be denoted as EC-3 (i.e. 3rd project funded by EC) or LCS-2 (i.e. 2nd project funded by LCS).

*) janis.spigulis@lu.lv

Biophotonics—Riga 2020, edited by Janis Spigulis, Proc. of SPIE Vol. 11585,
 · doi: 10.1117/12.2581799

Although a number of optical skin diagnostic devices are available on the market, many of them are suffering from insufficient reliability, comfort of use, self-sustainability and affordability in terms of costs. There is still deficit of devices able to provide objective (quantitative) diagnostic information based on the captured skin images. Most of our projects are aimed to fill this gap by developing experimental proof-of-concept prototype devices adapted for use in points-of-care, GP offices, clinics and hospitals, as well as being suitable for self-control in specific cases. Generally, the recent designs represent further developments of our previous prototype devices described in earlier review papers [2,3].

2. HYPERSPECTRAL-THERMAL IMAGER FOR EARLY DIAGNOSIS OF SEPSIS

A hybrid prototype device was developed in frame of the project EC-3 aimed at real-time inspection of skin blood hemoglobin saturation with oxygen (SO_2) maps overlapped with thermal images of diseased skin. The device can perform calculations in real-time and is suitable for bedside monitoring of septic patients.

The prototype (Fig.1) comprises three main modules: (1) hyperspectral imaging (HSI) system, (2) thermography (TG) system, and (3) computing-display (CPU) module. All components are installed in a tube and routable case. The HSI and TG systems are embedded at opposite ends of the tube housing. The CPU module with power supply and a touch-screen display are placed in a rectangular case on the side of tube between the HSI and TG systems; the CPU module can be turned over the horizontal axis for user convenience. The HSI system comprises illumination and detection modules. The illumination module involves a set of visible-spectrum LEDs (6 cyan LEDs CW = 505 nm/FWHM = 30 nm, 12 lime LEDs CW = 568 nm/FWHM = 100 nm), LED driver and 12-bit DAC controller which allows controlling the illumination intensity of all LEDs through the USB interface. All illuminator components are mounted on a printed circuit board. To provide uniform illumination of skin, a light diffusing film is placed between the LED ring and a linear polarizer film mounted at the output of illuminator. This system provides ~ 1 mW/cm^2 irradiance on the skin surface.

The detection module involves a compact snapshot HSI camera (XIMEA xiSpec MQ022HG-IM-SM4 × 4-VIS, 2048 × 1088 pix. snapshot, Fabry-Perrot interference filter 4 × 4 for 16 spectral bands in the range 470–630 nm, 10-bit ADC), which is equipped with near-field lens (8.5 mm, 2/3" f/1.4) allowing skin measurements from the distance of 7 cm. Linear polarizer film with orthogonal orientation relatively to the illumination polarizer (to eliminate skin glare) is mounted on the top of lens. The illumination intensity of each spectral band has been adjusted according to best-possible linearity of camera spectral sensitivity in the range of 500–625 nm. The field of view of the HSI system is round with diameter 50 mm, spatial resolution - 0.18 mm.

The TG camera (Xenics Gobi, Steemer Imaging, Puchheim, Germany, 640, 640 × 480 pix., 16-bit ADC, LWIR) is mounted on the other end of tube. The field of view of camera is 150 × 112 mm, spatial resolution is 0.23 mm. The entire

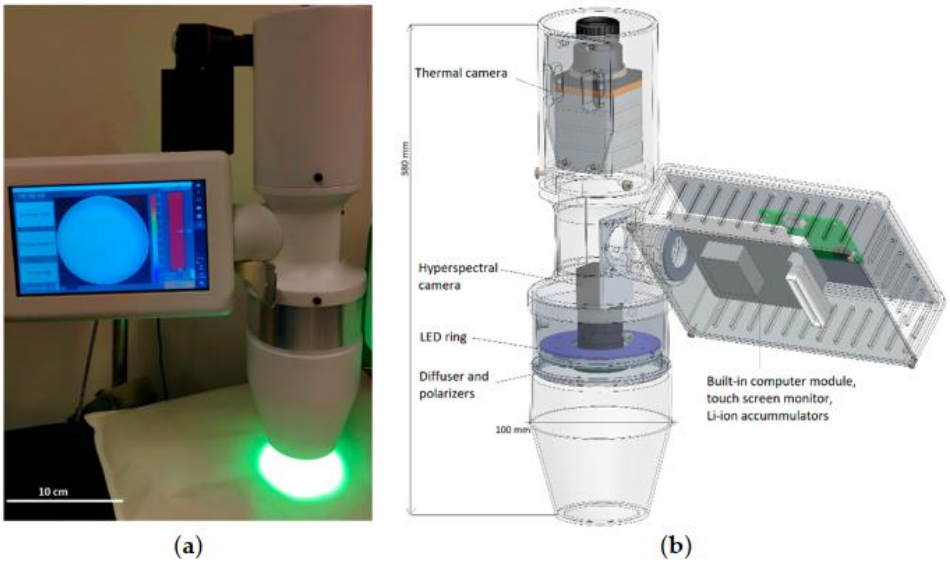

Figure 1. The hybrid prototype device in action (a) and its design scheme (b).

system can be controlled by built-in mini-computer (Windows-10 OS, CPU I-5, 16GB RAM, 512 GB SSD). A Graphical User Interface (GUI) developed in a Matlab environment allows controlling the device through a 7" touch-screen display. The Matlab GUI enables to preview skin images obtained from both cameras, to perform real-time calculations, and to visualize cutaneous blood SO_2 maps and skin temperature maps in color-coded image format, as well as to store data locally and remotely.

When turned on, the multimodal device starts software automatically, which works in two camera modes: (1) HSI mode, and (2) TG mode. In the HSI mode, the illuminator switches on (intensity ratio between the cyan and lime LEDs set to 1/20), and HSI camera becomes active. By the default, the video is displayed in color-coded format (r-g-b composite video) in preview mode. In the parametric mode, the saturation maps are displayed, also showing diagnostic parameters. In the TG mode, the thermal camera becomes active and the thermal video is displayed in the main window. Storing of data is performed by the user during the monitoring. Data acquisition time in HSI mode is 80 ms (12.5frames/s), processing time of blood oxygen saturation maps takes 1 s. The acquisition of TG data is performed at 25frames/s. More details on this prototype and its validation results can be found in [4].

3. DEVICE FOR EARLY NON-CONTACT DIAGNOSIS OF SKIN CANCER

This prototype (Fig.2) was created in frame of the EC-4 project, aimed at development and clinical validation of a novel portable device and cloud computing service for early diagnostics of melanoma and two other skin cancers (basal and squamous cell carcinomas), post-surgical scar follow-up and timely detection of tumor recurrence. Its initial versions were elaborated in our previous projects and reported in [5,6].

The device comprises a 5 Megapixel IDS camera and sequentially switchable sets of LEDs arranged in a ring. Light source includes three sets of narrow bandwidth LEDs with peak wavelengths 525 nm, 660 nm and 940 nm for spectral imaging of skin diffuse reflectance, as well as a 405 nm peaked LED to induce skin autofluorescence and a white broad-spectrum LED for capturing color images. As these multispectral illuminations reach a maximum power density of ~7mW/cm^2 and each wavelength exposure takes less than 2 seconds, the imaging method can be considered as non-invasive and harmless to the skin. In order to ensure homogeneous illumination and to eliminate any glare, a diffuser film and two crossed linear polarizers are placed in the system. It comprises also a 520 nm long pass filter, 4G cellular modem, WiFi dongle and Raspberry Pi Compute module for data processing and forwarding images to a cloud service.

Altogether four identical prototypes have been assembled to enable acquisition and transfer of a set of skin lesion images under specific illumination. Image processing software and cloud computing service (www.checkyourskin.eu) for distant

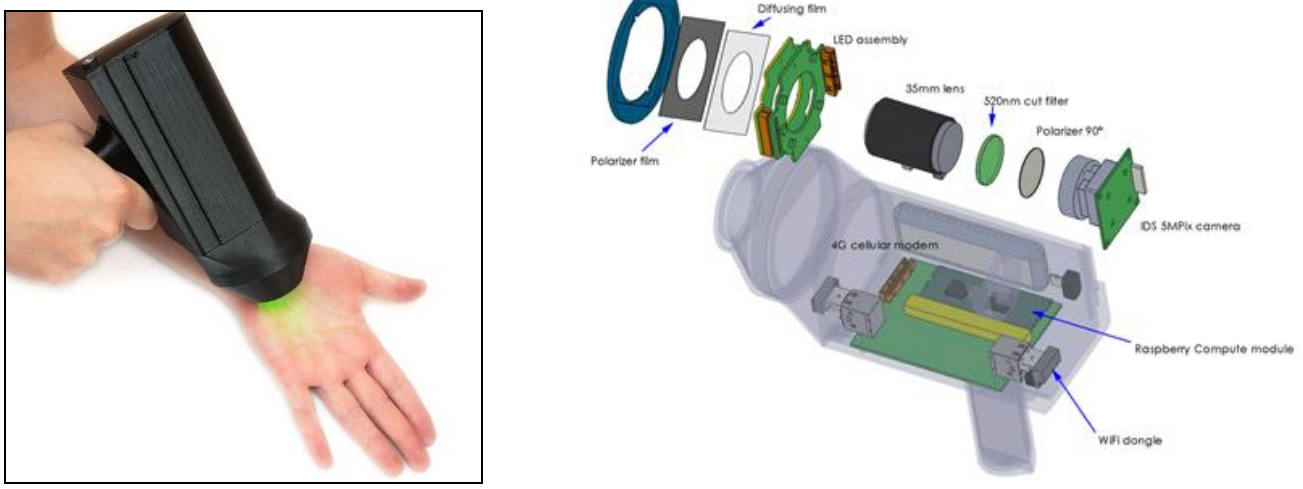

a b

Figure 2. The prototype for skin cancer detection in action (a) and its design scheme (b).

image processing and access to diagnostics results have been developed, too. The software performs automatic image processing including automatic segmentation of skin malformations, automatic calculation and mapping of a melanoma diagnostics criterion and the autofluorescence parameters. As part of the synergy, in the EC-7 project the previously developed empiric diagnostic criterion p' [7] was calculated from diffuse reflectance images at three wavelength bands and analyzed for melanoma diagnostics in combination with the criterion I` - ratio of the mean neoplasm autofluorescence intensity to that of the surrounding healthy skin [8-10]. Combination of two criteria - $p' > 1$ and $I` < 0.2$ – resulted in high accuracy (90%), with melanoma diagnostics sensitivity 85% and specificity 95% [9]. In addition, an autofluorescence based method has been elaborated for postoperative monitoring of surgical scars to help diagnosing the recurrence of skin cancer from the early stage of scar development [11].

The four equal prototypes were tested on different groups of malignant and benign lesions at Oncology Center of Latvia, Semmelweis University Department of Dermatology, Dermatooncology (Budapest, Hungary) and University Hospital "Tsaritsa Yoanna-ISUL" (Sofia, Bulgaria). A set of RGB and autofluorescence (AF) *in vivo* images that comprises 1508 skin malformations (Table 1) has been collected. Besides, a general practitioner (GP) in Latvia tested one of the

Table 1. Statistics of the measured skin neoplasms during validation of the prototype.
BCC – Basal Cell Carcinoma, SCC – Squamous Cell Carcinoma, Suspicious lesions – diagnosis has not yet been approved or the lesion has been left for observation until the next clinical check-up.

Diagnosis	Number
Malignant	**255**
Melanoma (Histology)	38
Melanoma (Citology)	2
Melanoma (Clinical)	6
Lentigo maligna	2
Dysplastic nevus	26
BCC	167
SCC	10
Kaposi sarcoma	1
Cutaneous metastasis	5
Actinic keratosis	7
Suspicious lesions	**64**
Benign	**877**
Blue nevus	7
Reed/Spitz nevus	1
Another pigmented nevus	405
Hyperkeratosis	77
Seborrheic keratosis	113
Vascular	39
Other	234
Postoperative scars	**312**
After melanoma	45
After BCC	170
After SCC	5
Other	92
Total	**1508**

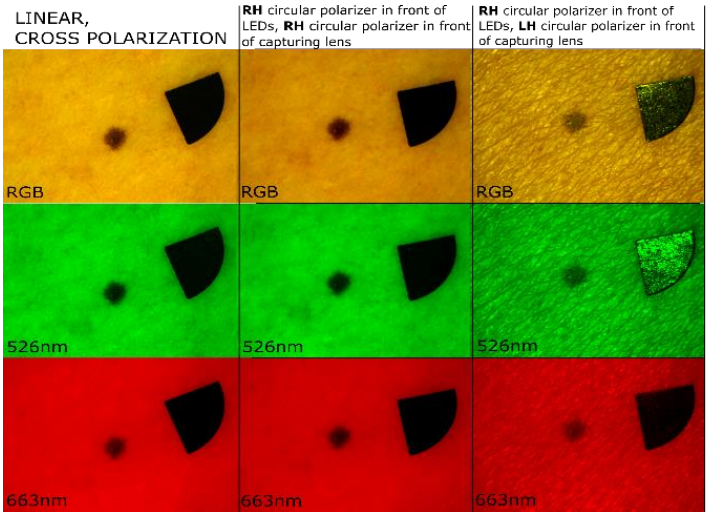

Figure 3. Comparison of polarization techniques for pigmented nevus imaging using white, green and red illumination.

prototypes and the data transfer service. In general, doctor evaluated the prototype and diagnostic service as valuable, innovative tool for screening of skin neoplasms in GP practice and acknowledged that the use of such service is much more convenient for patients and also much cheaper than visiting a dermatologist.

This study was extended in frame of the project EC-7 where a performance test replacing the crossed linear polarizers in the device by a couple of circular polarizers was done. Using uni-directional circular polarizers (two right-handed (RH) or two left-handed (LH)), similar results as with orthogonally oriented linear polarizers were obtained, while contra-directional couple of polarizers ensured notably better image resolution (Fig.3). As linear polarizers should be positioned at a perfect 90-degree angle which is sometimes not easy to adjust in systems, circular polarizers do not require a precise positioning angle and therefore seem to be preferable in the future designs.

The image processing technique was further developed in frame of the project LCS-2 where neural networks were trained by a synthesized multispectral data set. Identification of cutaneous melanoma this way requires a large amount of such data. Since the International Skin Imaging Collaboration (ISIC) archive consists of dermatological skin lesion images recorded only under white illumination, skin melanoma images were synthesized using multispectral images of nevi; the lesions were segmented and extracted from the rest of images. Using the gamma adjusting function, backscattered light intensity of the benign lesion was adjusted to depict new intensity range. After darkening, the

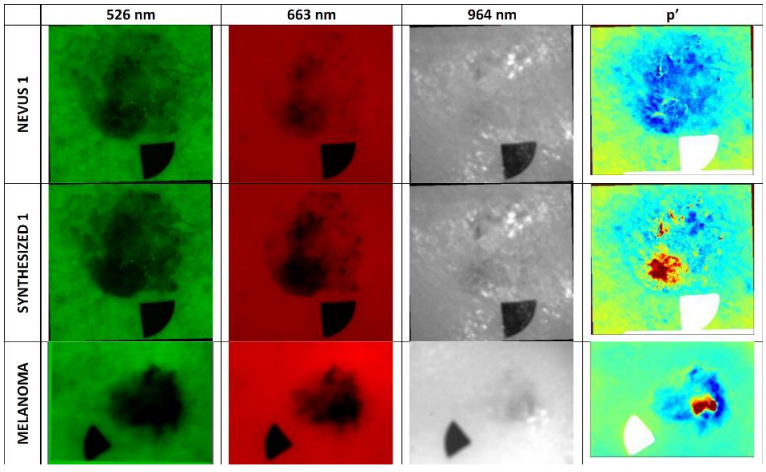

Figure 4. Spectral (526 nm, 663 nm, and 964 nm) images and melanoma diagnostic criterion *p'* map of several dermatologically approved nevi, correspondingly synthesized melanoma and histologically approved melanoma for comparison.

boundaries of the acquired segment were blended with the background skin to make the image look more realistic. The synthesized melanomas contained areas where the diagnostic criterion was $p' > 0$; this way spectral data set of ~ 300 melanomas was synthesized. A sample of real nevus, melanoma and synthesized melanoma images is shown in Fig. 4. Next, based on the synthesized data, a skin lesion classifier to find the most sensitive wavelengths for melanoma diagnosis was developed. Several neural network architectures were tested; the most sensitive imaging wavelengths appeared to be 450 nm, 590 nm and 950 nm. More details on the findings of last two projects can be found in [12-15].

4. PROTOTYPES FOR MULTI-SPECTRAL-LINE IMAGING OF SKIN

A few years ago we proposed and tested a new multispectral imaging modality where illumination of the target (e.g. skin) is performed by multiple laser-emitted spectral lines instead of spectral bands. Single spectral line image is acquired if only one spectral line is used for target illumination. We have demonstrated that up to three spectral line images can be extracted from a single snapshot RGB image data set under simultaneous triple-wavelength illumination [16-20]. The multi-spectral-line imaging (MSLI) concept was successfully implemented in several experimental prototypes that have passed tests for clinical and forensic applications [21-23]. This technology was further developed in the projects EC-8 and LCS-4.

Recently a four spectral line imaging double-camera prototype (Fig.5,a) was designed, assembled and tested [21]. Illumination system comprised two laser modules (1) – RGB module emitting ~ 20 mW at each of the three spectral lines (450 nm, 523 nm, 638 nm) and a NIR 850 nm / 40 mW module. As a patented novelty, several semi-elliptical loops of side emitting optical fiber (2) attached to the laser modules were exploited as light source ensuring uniform multi-laser illumination of the target area via a polarizing film. Two cameras - RGB and NIR (3), equipped with polarizers oriented orthogonally to the polarization direction of illumination (to suppress the surface-reflected light) were simultaneously capturing images of the same skin area. Four spectral line images were then extracted, displayed on the touch screen (4) and transferred via *wi-fi* to external computer for further calculation of chromophore distribution maps.

Another recent design [24] allowed consecutive capturing of five spectral line images within 4 seconds using a laser diode ring illuminator (Fig.5,b). Device (Fig.5,c) is based on *Windows CE 7.0* operating system; it has built-in processing software for nearly real-time calculation of skin chromophore maps. In total, 20 laser diodes emitting at five wavelengths (405, 450, 520, 660, and 850 nm) and 4 white LEDs for preview mode are operated. Each set of equal lasers is powered separately by a constant current laser driver. A system on chip module *Nvidia Tegra 2 T20* with a 1 GHz dual core *ARM Cortex-A9* processor is used as a central processing unit. 3 Mpix RGB CMOS matrix serves as the image sensor, connected to a central processor via a 10-bit parallel line. The image sensor has 10-bit ADC which provides1024 grades of intensities for each spectral image. Mini USB connector and SD memory card are used for image transfer to external computer. All low level tasks are laid down to 32-bit Arm-based *Cortex®-M4 STM32L4* series microcontroller. It is programmed as I2C interface slave device and emulates RTC chip. Pushbutton tasks are embedded in software. Dimensions of the device are 121 x 205 x 101 mm, weight ~ 440 g.

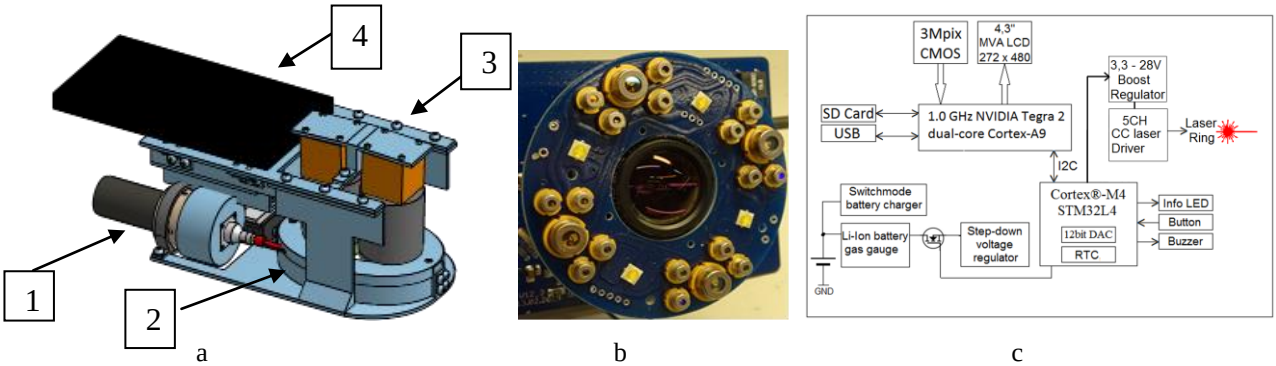

a b c

Figure 5. Design details of the recent four (a) and five (b,c) spectral line imaging prototypes [21,24].

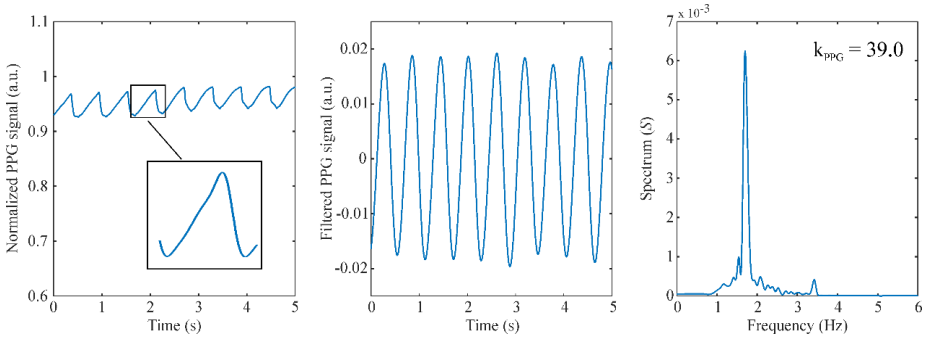

Figure 6. An example of good canine pulse oximeter signal (metacarpus, PR = 101bpm), filtered signal (band-pass filter frequencies of 1Hz and 3Hz) and its frequency spectrum for kurtosis (k_{PPG}) estimation.

5. DEVELOPMENT OF VETERINARY BIOPHOTONICS: THE FIRST STEPS

Currently, biophotonic techniques like various cameras, pulse oximeters, etc., remain rarely exploited in veterinary medicine. Only if a specific human system can be directly or with minor adjustments applied to animals, it gets used in the veterinary practice. In the project EC-2, we wanted to address some of the clinical challenges in medicine of dogs and cats by applying biophotonic techniques. We believe that biophotonic diagnostic techniques can help veterinarians and, by that, improve the health and well-being of dogs and cats.

Due to extensive pigmentation and hairiness of dogs and cats, a pulse oximeter, which monitors heart rate and blood oxygen saturation, is routinely placed solely on the tongue. Therefore, this approach is feasible only for unconscious dogs and cats, e.g., during surgical procedures. In our study, we investigated several other measurement sites (e.g., legs, tail) that could be tolerated by conscious animals (Fig.6). We discovered that the canine metacarpus and tail can be substituted for oral pulse oximeter placement since both measurement sites exhibited a high pulse oximeter signal kurtosis and were considered well-tolerated. On the other hand, the digit could be used in cats with some limitations. Additionally, the modified pulse oximeter device could measure animal capillary refill time (CRT), which is an essential parameter for estimating pet cardiovascular health.

Atopic dermatitis is a common canine inflammatory and pruritic skin disease associated with an allergy. The monitoring of skin erythema over time is an essential diagnostic need. Currently, the erythema assessment is done subjectively by visual estimation. In our work, we developed and tested a few optical devices (Skimager- and smartphone-based) for assessing canine skin objectively. We discovered that the correlation and the coefficient of determination between visual and objective erythema estimations were high (around 0.80). We concluded that optical measurements could replace the visual estimation of erythema in atopic dogs and, thus, improve the validity of skin lesion severity scales in dogs.

Results of our recent studies on veterinary biophotonics are published in [25-30].

6. EXPERIMENTAL STUDIES OF REMITTED PHOTON PATH LENGTHS IN SKIN

Values of the skin-remitted photon path lengths at particular wavelengths and input-output distances are important for several clinical applications including reflection pulse oximetry and skin chromophore mapping. The remitted photon path lengths in human skin can be estimated by modelling; however, there are very few experimental data available to validate the simulations. Models mostly consider distribution of path lengths for all photons independently of their travel directions and interactions within the tissue. One can expect that the mean path length of the survived skin-remitted photons should be longer than that related to all photons launched in the tissue (were a certain amount of them is absorbed). Systematic experimental studies on spectral and spatial dependencies of the skin-remitted photons are needed to quantitatively answer this question.

This study, performed in synergy of projects EC-1 and EC-6, exploited the photon time of flight method where picosecond laser pulses at seven wavelength bands (FWHM = 10 nm) in the spectral range 560-800 nm were launched into *in-vivo* forearm skin of 10 volunteers via an optical fiber. The pulses of back-scattered light were detected via another optical fiber placed at variable distance (1, 8, 12, 16 or 20 mm) from the input fiber, with subsequent analysis of their shapes for all 35 spectral-spatial combinations. Using a deconvolution algorithm, the distribution functions of

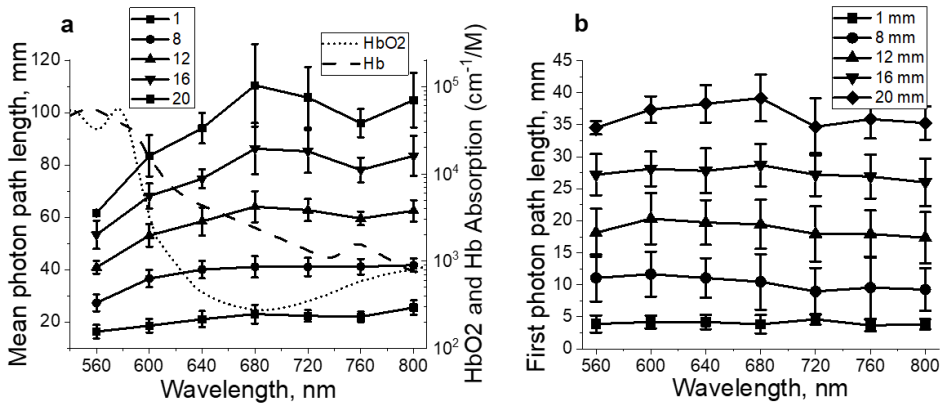

a b

Figure 7. a - spectral dependencies of the mean path length of skin-remitted photons at various inter-fiber distances, b – spectral dependencies of the path lengths calculated for the first-arrived photons (detected at 5% level of output pulse maximum). The dotted curves in (a) represent oxy- and deoxy-hemoglobin absorption (in logarithmic scale).

remitted photon arrival times after infinitely narrow input pulse were calculated and transformed into distributions of skin-remitted photon path lengths.

Nearly linear dependences of the remitted photon mean path length on inter-fiber distance were obtained for all wavelength bands, while the spectral dependences at fixed inter-fiber distances showed more complicated character, most probably due to absorption of the dermal hemoglobin (Fig.7). More details of this study are published in [31].

7. STUDIES OF CELL AUTOFLUORESCENCE PHOTO-BLEACHING

The mechanism of tissue autofluorescence photo-bleaching is still unclear. The main hypotheses considered in literature are: a) spontaneous fluorophore decomposition (after a number of absorption/emission cycles), b) destructive interactions with other dye-molecules and c) due to interaction with oxygen molecules and their derivatives. To check the hypothesis that intrinsic fluorophores of cells (NADH, flavines and lipopigments) play role as endogenous photosensitizers with subsequent production of singlet oxygen [32], in-vitro mouse melanoma cells B16F10 with attached singlet oxygen fluorescence sensor (SOSG) were irradiated by continuous laser irradiation (405 nm, power density 30 mW/cm2) within 10 minutes. The obtained in project EC-6 results (Fig.8.) demonstrate opposite trends of both fluorescence intensities over time. The decrease of cell's autofluorescence intensity can be well described by exponential decay with the rate constant τ_1 = 1.06 +/- 0.19 minutes while the SOSG fluorescence intensity increase was also exponential but slower, with the rate constant τ_2 = 2.6 +/- 1.15 minutes. One can assume that not only singlet oxygen is produced during the bleaching but also radicals such as hydroxyl radicals, superoxide anion radicals, etc.

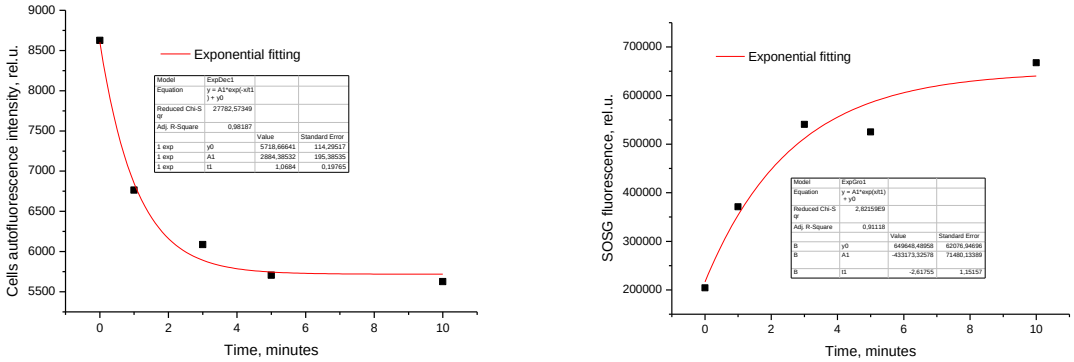

Figure 8. Left – melanoma cell autofluorescence intensity decrease during 10 minutes at 405nm continuous excitation measured at 480 nm band. Right – singlet oxygen fluorescence measured at 520nm band under 473nm excitation in the same experiment.

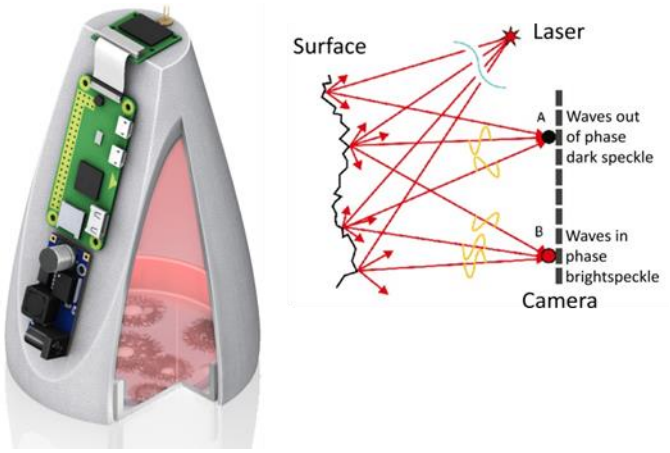

Figure 9. The proof-of-concept device with embedded ANN system for estimation of microbial activity by burst acquisition of laser speckle images (left) and scheme of the speckle pattern detection (right).

Obtained results support the concept that photo-bleaching occurs due to interaction with oxygen molecules and their derivatives. During the photo-bleaching process, illuminated cells (most likely also tissues) generate reactive oxygen species that lead to quenching of autofluorescence. Thus, violet/blue excitation causes an oxidative stress of the exposed cells and tissues, therefore long term illumination for diagnostics seems to be unsafe. On the other hand, this could be a good option to non-invasively provoke oxidative stress in tissues with subsequent measuring of fluorescence recovery time to provide information on tissue "wellness" (metabolic activity) which may have a potential for cancer diagnostics.

8. LASER SPECKLE MONITORING OF MICRO-ORGANISM'S ACTIVITY

Enumeration of live microbial cells in the sample is one of the basic quantitative measurements in microbiology. To ensure fast estimation of total plate count, laser speckle method in combination with image correlation analysis can be used. Object which create speckle image has scattering properties, and change in these properties creates a time - varying speckle pattern, e.g. due to the growth of bacterial colonies on this surface. In the project LCS-3, laser speckle patterns were captured by a CMOS sensor during illumination of growing bacteria colonies under illumination by low power (<30 mW, 635 nm) stabilized laser diode. The assembled cost-effective proof-of-concept prototype device is illustrated in Fig.9. Due to mass produced electronics, the total price of the device is only ~50 EUR (12 EUR – Raspberry Zero W, 20 EUR – Raspberry Camera, 6 EUR – laser diode, 10 EUR – PCB). To validate the proposed technique and image processing algorithm, fast growing *vibrio natriegens* bacteria were used. In order to quantify the changes in the speckle image appearing as a result of dynamic activity that occur over time, a two-dimensional normalized correlation between the image fragment before and after the event appearance is performed. Detailed description of the laser speckle time variable image processing is available in [33].

9. SUMMARY

To summarize, a number of high-priority projects are running or have been completed in the Biophotonics Laboratory over the recent three years. The project topics are mainly related to camera-based non-contact assessment of in-vivo skin malformations or microcirculation dysfunctions, aiming at development of novel devices and technologies for improved clinical diagnostics and recovery monitoring. Two new research directions – on biophotonics applications in veterinary medicine and in cell biology - have been initiated during this period. The above-reported results confirm the promising potential of optical methods for better health care of humans and pets. Several of the new prototypes have reached TRL of 4 or 5, so efforts in future should be put on the technology transfer aiming at commercialization of the developed new prototype devices and technologies for benefit of patients and health care professionals.

ACKNOWLEDGEMENTS

The above-described research was supported by the European Commission program "Horizon 2020" (projects #871124 "Laserlab-Europe" and #745396-DogSPEC-H2020-MSCA-IF-2016 "DogSpec") and European Regional Development Fund (projects #1.1.1.1/16/A/065 "Optical noninvasive hybrid method for early diagnostics of sepsis and therapy management", #1.1.1.1/16/A/197 "Portable device for early non-contact diagnostics of skin cancer", #1.1.1.1/18/A/132 "Multimodal imaging technology for in-vivo diagnostics of skin malformations, #1.1.1.2/VIAA/1/16/014 "Time-resolved autofluorescence methodology for non-invasive diagnostics of skin cancer", #1.1.1.2/VIAA/1/16/052 "Development and clinical validation of a novel cost effective multi-modal methodology for early diagnostics of skin cancers" and #1.1.1.2/VIAA/1/16/070 "Development of prototype devices for nonivasive assessment of skin condition"), as well as by the Latvian Council of Science (projects # lzp-2018/2-0052 "Improving the early diagnosis of skin cancer with neural networks", # lzp-2018/2-0051 "Fast and non-contact optical estimation of microorganisms activity" and # lzp-2018/2-0006 "Advanced spectral imaging technology for skin diagnostics").

REFERENCES

[1] "Biophotonics—Riga 2017", SPIE Proceedings, vol.10592 (2018). Editor: Janis Spigulis. https://spie.org/Publications/Proceedings/Volume/10592.
[2] Spigulis J., "Biophotonic technologies for noninvasive assessment of skin condition and blood microcirculation", Latv.J.Phys.Techn.Sci., **49**(5), 63-80 (2012).
[3] Spigulis J., "Multispectral, fluorescent and photoplethysmographic imaging for remote skin assessment", Sensors, **17,** 1165 (2017).
[4] Rubins U. et al., "Multimodal device for real-time monitoring of skin oxygen saturation and microcirculation function", Biosensors, 9, 97 (2019).
[5] Spigulis J .et al., "SkImager: a concept device for in-vivo skin assessment by multimodal imaging", Proc.Est.Acad.Sci., **63**(3), 213-220 (2014).
[6] Jakovels D .et at., "Benign-atypical nevi discrimination using diffuse reflectance and fluorescence multispectral imaging system", Proc. BioPhotonics 2015 (Florence, IT), 7304026 (2015). https://ieeexplore.ieee.org/document/7304026.
[7] Diebele I. et al., "Clinical evaluation of melanomas and common nevi by spectral imaging", Biomed.Opt.Express, **3**(3), 467-472 (2012).
[8] Lihacova I. et al., "A method for skin malformation classification by combining multispectral and skin autofluorescence imaging", Proc. SPIE **10685**, 1068535 (2018).
[9] Lukinsone V. et al., "Multispectral and autofluorescence RGB imaging for skin cancer diagnostics", Proc. SPIE **11065**, 110650A (2019).
[10] Lihachev A. et al., "Differentiation of seborrheic keratosis from basal cell carcinoma, nevi and melanoma by RGB autofluorescence imaging," Biomed Opt Express **9**(4), 1852-1858 (2018). DOI 10.1364/BOE.9.001852.
[11] Tamosiunas M. et al., "Autofluorescence imaging for recurrence detection in skin cancer postoperative scars", J.Biophot. **13**(3), e201900162, 2020.
[12] Bolochko K. et al., "Quality enhancement of multispectral images for skin cancer optical diagnostics," SPIE Proc 10679, 1067903 (2018). DOI 10.1117/12.2306609.
[13] Bolochko K. et al., "Towards to deep neural network application with limited training data: synthesis of melanoma's diffuse reflectance spectral images", Proc. SPIE **11074**, 110741O (2019).
[14] Bliznuks D. et al.,"Identification of the most informative wavelengths for non-invasive melanoma diagnostics in spectral region from 450 to 950 nm," Proc. SPIE **11459**, 114590K (2020).
[15] Bondarenko A. et al., "Use of machine learning approaches to improve non-invasive skin melanoma diagnostic method in spectral range 450 - 950nm", Proc. SPIE **11353**, 113531D (2020).
[16] WO 2013135311 A1 (2012). Method and device for imaging of spectral reflectance at several wavelength bands. (J. Spigulis, L. Elste).
[17] Spigulis J. et al., "Towards single snapshot multispectral skin assessment", Proc. SPIE **8216**, 82160L (2012).
[18] Spigulis J., Elste L., "Single-snapshot RGB multispectral imaging at fixed wavelengths: proof of concept", Proc. SPIE **8937**, 89370L (2014).
[19] Spigulis J. et al., "Smartphone snapshot mapping of skin chromophores under triple-wavelength laser illumination", et al., J.Biomed.Opt., **22**(9), 091508 (2017).
[20] Spigulis J**.** et al, "Snapshot multi-spectral-line imaging for applications in dermatology and forensics", Proc.SPIE **10881**, 1088114 (2019).
[21] Spigulis J. et al., "A snapshot multi-wavelengths imaging device for in-vivo skin diagnostics", Proc.SPIE **11232**, 112320I-1 (2020).

[22] LV 15106 B (2016) “Method and device for mapping of chromophores under illumination by several laser lines” (J.Spigulis, I.Oshina).
[23] Oshina I. et al., “Express RGB mapping of three to five skin chromophores”, Proc. SPIE-OSA **10413**, 104130M-1 (2017).
[24] Kviesis-Kipge E., “Development of skin chromophore mapping device using five spectral line illumination”, OSA Technical Digest (2019), ITh4B.3, https://doi.org/10.1364/ISA.2019.ITh4B.3.
[25] Cugmas B., Spigulis J., “Biophotonics in veterinary medicine: the first steps toward clinical translation”, Proc.SPIE **10885**, 108850I (2019). DOI: 10.1117/12.2507980.
[26] Cugmas B., Štruc E., Spigulis J., “Photoplethysmography in dogs and cats: a selection of alternative measurement sites for a pet monitor”, Physiol. Meas., **40**, 01NT02 (2019). DOI: 10.1088/1361-6579/aaf433.
[27] Cugmas B. et al., “Photoplethysmography for bovine heat detection: the preliminary results”, Proc.SPIE **11247**, 112470J (2020). DOI: 10.1117/12.2543858.
[28] Cugmas B., Štruc E., Spigulis J., “Clinical evaluation of automated capillary refill time estimation in dogs and cats”, Proc.SPIE **10868,** 108681N (2019). DOI: 10.1117/12.2507620.
[29] Cugmas B., Spigulis J., “Challenges in automated estimation of capillary refill time in dogs”, Proc. SPIE **10501**, 1050117 (2018). DOI: 10.1117/12.2284794.
[30] Cugmas B. et al., “Skimager for the objective erythema estimation in atopic dogs”, Proc. SPIE **11211**, 1121110 (2020). DOI: 10.1117/12.2544664.
[31] Lukinsone V.et al., “Remitted photon path lengths in human skin: in-vivo measurement data”, Biomed.Opt.Expr. **11**(5), 2866-2873 (2020). https://doi.org/10.1364/BOE.388349.
[32] Plavskii V.Yu. et al., “Porphyrins and flavins as endogenous acceptors of optical radiation of blue spectral region determining photoinactivation of microbial cells”, J.Photochem.Photobiol., **B183**,172-183 (2018).
[33] Balmages I. et al., "Laser speckle time-series correlation analysis for bacteria activity detection", Proc. SPIE **11359**, 113591D (2020). https://doi.org/10.1117/12.2541663.